Characteristics and sources of halogenated hydrocarbons in the Yellow River Delta region, northern China

Penggang Zheng[a], Tianshu Chen[a], Can Dong[a,*], Yuhong Liu[a], Hongyong Li[a], Guangxuan Han[b], Jingjing Sun[a], Lin Wu[a], Xiaomei Gao[c], Xinfeng Wang[a], Yanbin Qi[d], Qingzhu Zhang[a], Wenxing Wang[a], Likun Xue[a,e,*]

[a] Environment Research Institute, Shandong University, Qingdao, Shandong, China
[b] Key Laboratory of Coastal Environmental Process and Ecology Remediation, Yantai Institute of Coastal Zone Research, Chinese Academy of Sciences, Yantai, Shandong, China
[c] School of Water Conservancy and Environment, University of Ji'nan, Ji'nan, Shandong, China
[d] Jilin Weather Modification Office, Changchun, Jilin, China
[e] Ji'nan Institute of Environmental Science, Ji'nan, Shandong, China

ABSTRACT

As important ozone-depleting substances and potential greenhouse gases, halocarbons have attracted much attention since 1970s. To better understand the characteristics and sources of halocarbons in the Yellow River Delta (YelRD) region, an important oil extraction and petrochemical industrial area in northern China, a two-phase (winter-spring and summer) intensive campaign was conducted in 2017. Compared with the Northern Hemispheric background, median enhancements of Montreal Protocol (MP) regulated species (CFCs, Halons and CH_3CCl_3) in this region were relatively small. Meanwhile, enhancements were relatively large for MP under control species (HCFCs and HFC-134a). Historical trends of halocarbons in China and the YelRD region both exhibited declining and increasing trends for MP regulated and under control species, respectively. Results above indicate effective implementation of MP in China. The enhancements of MP unregulated species were high as they are still used and uncontrolled. In addition, oil fields were found to have a negligible influence on ambient halocarbons in this region. The back-trajectory analysis shows that clusters from the North China Plain and East China were associated with the highest concentrations of most halocarbons during the winter-spring and summer periods, respectively. Source apportionment of halocarbons was carried out by positive matrix factorization (PMF). Model results indicate that biomass burning, marine, refrigerants and foam blowing, and solvent usage were the most important sources. This study provides the underlying insights into the characteristics and sources of halocarbons in the YelRD region.

1. Introduction

Since Molina and Rowland (1974) revealed the mechanism of chlorine atom catalysed destruction of stratospheric ozone in 1970s, halocarbons have got extensive attention as ozone depleting and global warming substances (IPCC/TEAP, 2005). Halocarbons can be divided into several sub-classes, including chlorofluorocarbons (CFCs), Halons, hydrochlorofluorocarbons (HCFCs), hydrofluorocarbons (HFCs), and some short-lived halogenated substances (a broad class of chlorine- and bromine-containing substances known as very short-lived halogenated substances (VSLSs) that have lifetimes shorter than about 6 months and are not controlled under the Montreal Protocol). CFCs, along with

CH_3CCl_3 and CCl_4 were widely used in the pre-MP era (prior to the signing of the Montreal Protocol) as refrigerants, closed-cell foam plastics, aerosol propellant, medical aerosol products, solvents, and industrial applications (Artuso et al., 2010; McCulloch and Midgley, 2001; McCulloch et al., 2003; Sturrock, 2002). Due to their long lifetimes, CFCs can be transported to the stratosphere where they could be photolyzed to release the highly reactive chlorine/bromine atoms and destroy ozone (WMO, 2014). Halons were also widely applied in the pre-MP era as fire extinguish agents in domestic, commercial and military applications (Montzka et al., 1999). However, the ozone depletion potentials (ODPs) of Halons are significantly larger than that of CFCs because bromine is much more effective (about 60 times) in
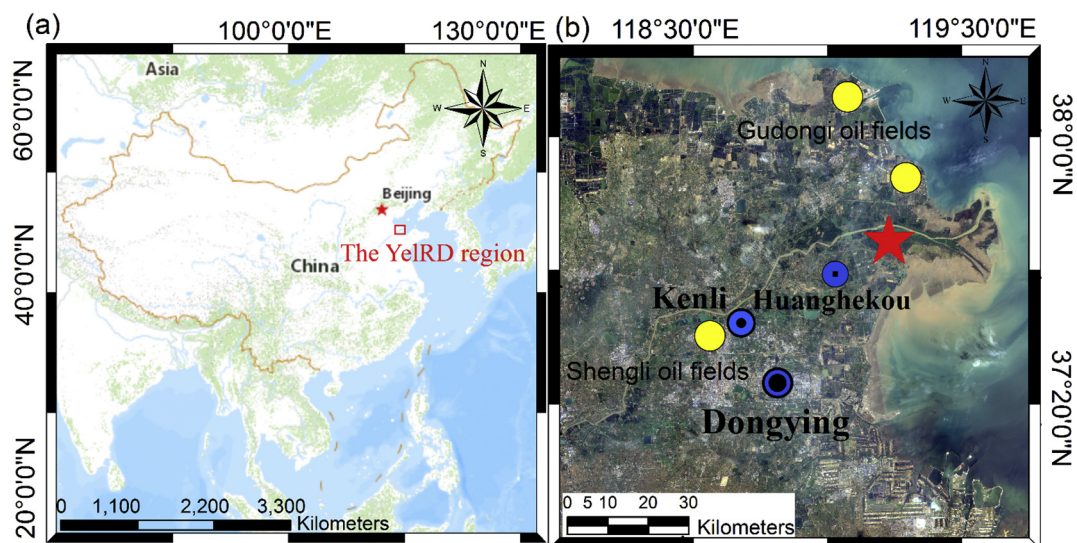

Fig. 1. (a) Location of the YelRD region (boxed area), (b) Locations of the sampling site (red star), oil fields (yellow dots), and adjacent cities and towns (black dots indicate the size of the city/town). (For interpretation of the references to colour in this figure legend, the reader is referred to the web version of this article.)

destroying ozone (WMO, 2014). In the past few decades, HCFCs were increasingly used in refrigeration, air conditioning and foam plastics to replace CFCs for their lower ODPs (Kim et al., 2011). Meanwhile, HFCs have nearly zero ODPs and thus are considered as better substitutes for CFCs and HCFCs (O'Doherty et al., 2004). Despite of their differences in ODPs, all the aforementioned halocarbons are greenhouse gases and were estimated to contribute positive globally averaged radiative forcing (IPCC/TEAP, 2005). Moreover, most of the VSLSs are toxic to human (Simmonds et al., 2006) and some VSLSs may also contribute significantly to ozone loss in the stratosphere (Fang et al., 2018a).

After realizing the environmental effects of halocarbons, a series of treaties, including *Montreal Protocol on Substances that Deplete the Ozone Layer* and its amendments, were contracted to control the ODSs. After years of control, the overall abundances of ODSs in the global atmosphere have kept decreasing for more than a decade (WMO, 2014). Levels of CFCs, CCl_4, CH_3CCl_3, and H-1211 (Halon 1211) continue declining, while H-1301 is expected to maintain a certain level due to its continued small releases and long lifetime (65 years). CH_3Br concentrations have decreased by 98% compared to its peak levels (WMO, 2014). Concentrations of HCFCs are still increasing, but total emissions of major HCFCs have declined as a result of the implementation of MP. HFCs have been increasing at a relatively rapid rate because of great application demands (WMO, 2018). Nevertheless, some unexpected phenomena also occurred. Although CFC-11 mixing ratios are still declining, its emissions may have increased in recent years (Montzka et al., 2018). Lunt et al. (2018) found continued emissions of the CCl_4 from eastern Asia. Unexpected emissions of CFC-113, CFC-114 and CCl_4 after 2012 were reported (WMO, 2018). A recent study reported that if emissions of $CHCl_3$ (chloroform, belonging to VSLSs) continue to grow at the recent rate, future ozone-layer recovery could be delayed by several years (Fang et al., 2018a). In summary, the implementation of MP is effective, but we should still be vigilant for unexpected emissions and their environmental impacts.

China has made great progress on the phase-out of halocarbons and eliminated more than 100,000 tons of ODSs in the past 30 years (Fang et al., 2018b). With all ODSs being phased out on schedule, CFCs, Halons and CCl_4 were even eliminated in advance in 2007 (Wu et al., 2018). Previous studies have reported the characteristics of halocarbons in China. Fang et al. (2012a) estimated that total emissions of CFCs and HCFCs were decreasing in China between 2001 and 2009. Two other studies showed that most of the halocarbons in 45 Chinese cities were only within 10% to 20% enhancements of the global background

(Barletta et al., 2006; Fang et al., 2012b). In an aircraft measurement over east Shandong Peninsula in 2011, CFCs, together with CCl_4 and CH_3CCl_3, showed slightly higher levels compared to the global background (Wang et al., 2014a). Zhang et al. (2017) reported that CFCs showed a decreasing trend at four regional background sites of China. However, such studies became relatively rare after 2012 in China. Since the phasing out of HCFCs in China carried out in 2013, more research about halocarbons is urgently needed.

With a population of about 10 million people, the Yellow River Delta (YelRD) region is the second largest estuary delta region in China. Adjacent to the Bohai Sea, the YelRD region is located at the junction of Shandong Peninsula and Beijing-Tianjin-Hebei metropolitan area (the biggest urbanized region in Northern China). In the past 30 years, industrialization and urbanization of the YelRD region may have resulted in high pollution levels of halocarbons (Guo et al., 2009). Endowed with abundant oil and natural gas resources, many petrochemical industries which produce high levels of volatile organic compounds are located in this region. In addition, some marine source species (e.g., CH_3I, CH_3Br, etc.) could be abundant in the coastal sea area. Thus, a better characterization of the pollution features and sources of halocarbons in this area is needed. In this study, a two-phase intensive campaign was conducted in 2017. A total of 111 and 22 samples were collected at a field site and in oil fields (all located in the YelRD region), respectively, and 24 atmospheric halocarbon species were detected. In combination with the HYSPLIT back trajectory and positive matrix factorization (PMF), we report the characteristics and sources of halocarbons in this region. In addition, considering the fact that the published halocarbons data in China is a little lacking after 2012, we provide an overview of pollution levels of halocarbons in China. We also focused more on HCFCs, because their phase-out schedule was carried out in 2013 in China. In addition, our work can provide some implications for decision-makers.

2. Methods

2.1. Sampling site

The sampling site is in the Yellow River Delta Ecological Research Station of Coastal Wetland (37.75°N, 118.97°E, 1 m above sea level), which is located in the Yellow River Delta National Natural Reserve and is only 10 km away from the Bohai Sea (see Fig. 1). There are no densely populated and industrial areas within a distance of 10 km

around the station. Dongying City, Kenli District, and Huanghekou Town are three major cities or towns around. They are located 32 km, 42 km and 16 km to the southwest of the site, respectively. The Shengli Oil Field, which is the third largest oil field in China, surrounds the site, leaving only a narrow gap in the southeast. To sum up, the station is a complicated coastal rural site in oil fields that may receive different types of air masses which include oilfield air, marine air, urban plumes, and aged air masses transported over a long distance from the Beijing-Tianjin-Hebei region or East Asia. A detailed description of this study site is given in Zhang et al. (2019).

2.2. Sampling and laboratory analysis

A two-phase campaign was conducted in the winter-spring (from February 13 to April 3) and summer (from June 8 to July 9) of 2017. Two-liter pre-vacuumed, electro-polished, stainless-steel canisters from the University of California, Irvine (UCI) were used to collect whole air samples. During the sampling, the bellows valve of the canister was kept slightly open for 3 min to avoid the instantaneous air mass pollution. During the first 6 days of the winter-spring campaign, 2 samples were collected each day at 00:00 and 12:00 local time (LT). After February 18, 6 samples were collected each day, but only on polluted days (according to the air quality forecast from https://map.zq12369.com/) with a 3-h interval from 6:00 to 21:00 LT. In the summer campaign, 7:00, 10:00, 12:00, 14:00, 16:00 and 19:00 LT were chosen as the sampling time on polluted days. Additional 11 air samples were collected in the oil fields during each phase of the campaign. In summary, a total of 133 samples (64 for the winter-spring period and 69 for the summer period) were collected.

After the campaign, the canisters were sent back to UCI for composition and concentration analysis. The whole air samples were analysed by GC-FID/ECD/MS. Six column-detector combinations were used, which include two electron capture detectors (ECD, sensitive to halocarbons and alkyl nitrates), two flame ionization detectors (FID, sensitive to hydrocarbons), one quadrupole mass spectrometer detector (MSD, for unambiguous compound identification and selected ion monitoring) and one nitrogen phosphorus detector (NPD, for detection of nitrogen species). A total of 24 halocarbon species (see Table 1), DMS and CO were detected and analysed in this study. The accuracy and measurement precision vary by compound and are estimated to be 3–20% and 3–10%, respectively (Colman et al., 2001; Simpson et al., 2010). The limit of detection (LOD) also varies by compound, from 0.01 ppt for chlorobrominated species to 10 ppt for CFC-12 (Simpson et al., 2010). Detailed information about laboratory analysis, detector and precision of each compound can be found on the website of the Rowland-Blake Group (https://ps.uci.edu/~rowlandblake/research_lab.html) and is also given in the Supplementary material.

2.3. Backward trajectory analysis

The Hybrid Single-Particle Lagrangian Integrated Trajectory model (HYSPLIT, version 4.9; Draxier and Hess, 1998) developed by the National Oceanic and Atmospheric Administration (NOAA) Air Resources Laboratory (http://www.arl.noaa.gov/ready/hysplit4.html) was used to understand the air masses history in this study. The meteorological data were from the Global Data Assimilation System (GDAS) data set (http://ready.arl.noaa.gov/archives.php). Considering the long lifetimes of most detected halocarbons, 120-h back trajectories and associated clusters were performed and analysed. Three hundred meters above the ground level was chosen as the end point to avoid the influence of surface topography (Stohl et al., 2003). Back trajectories were restarted every 3 h (from 0:00 to 21:00 LT) and those corresponding to the sampling time were used for cluster analysis. The cluster analysis was performed with the HYSPLIT built-in cluster function which uses multivariate statistics to group the most similar trajectories into one category (Sun et al., 2016). Finally, the numbers of

clusters were selected according to the total spatial variance change in scree plot.

2.4. PMF receptor model

Positive matrix factorization (PMF5.0) was used for source apportionment of halocarbons (EPA, 2014). For this study, the model was driven by 111 site samples and 25 selected species (22 halocarbons, DMS, CO and the sum of all input species). DMS and CO were treated as marine and combustion indicators, respectively (Guo et al., 2009). H-1211 and CH_3CCl_3 were excluded from the model as they exhibited slightly lower levels than Northern Hemispheric (NH) backgrounds in the YelRD region. Possible reasons for their low values will be discussed in Section 3.1. CFC-114 was also excluded from the model because it displayed a non-normal curve in the model. Due to the long lifetimes of some halocarbons, the global and regional backgrounds have significant impacts on their concentrations. Thus, the global baseline subtraction method (subtracting global or hemispheric average values from observed concentrations) was used to eliminate this effect in this study (Guo et al., 2009; Li et al., 2014; O'Doherty et al., 2001). Prior to using the method, samples with extremely high and low values classified by Tukey's test were replaced with the measured median values. For species (CO, DMS, $CHBr_2Cl$, $CHBrCl_2$ and $C_2H_4Cl_2$) whose background concentrations are not available, the corresponding 5% percentile of site samples was used. After subtracting the NH background, negative values were replaced with half limit of detection (LOD) (Sarkar et al., 2018). The uncertainty of each value was given by (EPA, 2014):

$$Uncertainty = \sqrt{(ErrorFraction * concentration)^2 + (0.5 * LOD)^2} \qquad (1)$$

For negative values, uncertainties were estimated as 5/6 of LOD (Li et al., 2014).

After data pre-treatment as described above, different numbers of sources (from 2 to 10) were tested in the PMF model to find the optimal value for most reasonable results. Finally, 5 factors were chosen for both goodness-of-fit of the model and prior knowledge about halogenated compounds emissions (Li et al., 2014). Details of the identification of major sources and their contributions to the ambient air will be discussed in Section 3.3.

3. Results and discussion

3.1. General characteristics of halocarbons in the YelRD region

Table 1 shows the mixing ratios of measured halocarbons at the sampling site and in the oil fields. NH background values, *p*-values (for the differences between our study and the NH background), lifetime, ODPs and 100-year GWPs of each species are also listed. The NH background data were derived from the World Data Centre for Greenhouse Gases (WDCGG). Median values of measurements during February 13 – April 3 and June 8 – June 9 of 2017 at three NH sites, i.e. Trinidad Head (41.05°N, 124.15°E), Mace Head (53.32°N, 9.90°W), and Junfraujoch (46.55°N, 7.99°E), were used as the background. These background sites are located in the uninhabited mountains or capes of the Northern Hemisphere and are at similar latitude to that of the sampling site in this study. As shown in Fig. 2, the measured halocarbons are divided into 3 categories (MP eliminated species, MP under control species, and unregulated species) according to the Montreal Protocol. The first category includes CFCs, Halons, CH_3CCl_3, CCl_4 and CH_3Br. Median concentrations of H-1211 and CH_3CCl_3 in the YelRD region were comparable to the NH background, while the rest of the species in the first category showed slightly higher median concentrations (except CH_3Br and CCl_4). Low concentrations of MP eliminated species (except CH_3Br and CCl_4) in the YelRD region demonstrate effective emission reductions of them in China. The enhancement

Table 1

Statistics of major halocarbons measured at the sampling site and within oil fields, together with the NH background levels[a].

Species	Ambient air (n = 111)		Oil field (n = 22)	NH background[b]	P value [c] (between site and background)	Lifetime[d]		ODPs	100-year GWPs
	Winter - spring	Summer							
	Median (Mean ± 1σ)	Median (Mean ± 1σ)	Median (Mean ± 1σ)	Median (Range)		Summer	Winter		
CFC-12	530 (530 ± 12)	530 (529 ± 14)	535 (539 ± 20)	511 (510–518)	0.000	102y		0.82	10,300
CFC-11	257 (271 ± 57)	269 (274 ± 26)	283 (302 ± 79)	228 (227–229)	0.000	52y		1	5160
CFC-113	77 (77 ± 5)	82 (83 ± 5)	78 (78 ± 3)	73 (72–73)	0.000	93y		0.85	6080
CFC-114	16.4 (16.5 ± 0.5)	16.8 (16.9 ± 0.6)	16.9 (17.1 ± 1.0)	16.3 (16.3–16.3)	0.000	189y		0.58	7710
H-1211	3.6 (5.5 ± 7.7)	3.4 (3.5 ± 0.2)	3.4 (7.7 ± 18.7)	3.6 (3.6–3.6)	0.028	16y		7.9	4590
H-1301	3.5 (4.0 ± 3.7)	3.5 (3.6 ± 0.3)	3.5 (3.7 ± 0.5)	3.4 (3.4–3.4)	0.000	72y		15.9	6670
CCl$_4$	109 (129 ± 62)	106 (117 ± 37)	102 (110 ± 32)	81 (80–81)	0.000	26y		0.82	3480
CH$_3$Br	31 (68 ± 98)	17 (25 ± 23)	15 (22 ± 17)	7 (7–8)	0.000	0.8y		0.66	2
CH$_3$CCl$_3$	2.8 (2.9 ± 0.4)	2.6 (2.6 ± 0.1)	2.6 (2.6 ± 0.2)	2.7 (2.6–3.4)	0.198	5y		0.16	153
HFC-134a	104 (131 ± 100)	119 (122 ± 16)	120 (126 ± 28)	84 (81–97)	0.000	14y		0	1360
HCFC-22	371 (1113 ± 2932)	427 (464 ± 184)	460 (469 ± 175)	229 (225–247)	0.000	11.9y		0.04	1780
HCFC-142b	29 (31 ± 6)	33 (42 ± 36)	33 (36 ± 14)	22 (21 − 22)	0.000	18y		0.065	2070
HCFC-141b	36 (173 ± 564)	43 (45 ± 11)	46 (45 ± 12)	24 (24–26)	0.000	9.4y		0.11	800
CHCl$_3$	283 (476 ± 701)	260 (378 ± 310)	212 (452 ± 477)	12 (5–14)	0.000	97d	750d	–[e]	
CH$_2$Cl$_2$	396 (500 ± 389)	574 (723 ± 467)	614 (624 ± 474)	60 (60–63)	0.000	95d	725d		
C$_2$HCl$_3$	20 (149 ± 411)	24 (97 ± 360)	22 (52 ± 81)	3 (3–3)	0.159	4d	27d	0.0006	
C$_2$Cl$_4$	18 (50 ± 102)	21 (27 ± 20)	16 (30 ± 33)	4 (3–4)	0.000	58d	450d		
CH$_3$Cl	1106 (1752 ± 1630)	1242 (1879 ± 1336)	1368 (3783 ± 5777)	584 (573–603)	0.000	0.9y		0.02	11
CH$_3$I	2.0 (2.1 ± 0.9)	3.4 (3.8 ± 2.2)	3.5 (3.0 ± 1.6)	0.7 (0.5–0.8)	0.023	99d	780d	0.066	
CH$_2$Br$_2$	1.1 (1.3 ± 0.5)	1.1 (1.4 ± 0.9)	0.9 (1.0 ± 0.3)	0.9 (0.8–0.9)	0.222	80d	620d		
CHBrCl$_2$	1.6 (2.3 ± 2.5)	1.4 (1.8 ± 1.2)	1.3 (2.0 ± 1.7)			56d	410d		
CHBr$_2$Cl	1.3 (1.9 ± 1.8)	1.2 (1.4 ± 1.0)	0.8 (1.5 ± 1.4)			43d	310d		
CHBr$_3$	3.9 (5.7 ± 4.4)	3.6 (4.8 ± 3.6)	2.5 (4.0 ± 4.2)	0.7 (0.6–0.9)	0.097	34d	250d	0.216	
C$_2$H$_4$Cl$_2$	480 (732 ± 717)	370 (586 ± 511)	238 (334 ± 304)			41d	320d		

[a] Units are in ppt.

[b] Using the latest data that can be obtained for the three NH background sites (Trinidad Head (41.05°N, 124.15°E), Mace Head (53.32°N, 9.90°W), Junfraujoch (46.55°N, 7.99°E)), the NH background medians were calculated for dates February 13 – April 3 and June 8 – June 9 of 2017, which is consistent with the sampling time of this study. The year of the background data is species dependent, ranging from 2008 to 2017.

[c] The *p*-value between NH background and YelRD region is calculated after excluding outliers with Tukey's test.

[d] The atmospheric lifetime, ODPs, GWPs of halogenated hydrocarbons are from the Scientific Assessment of Ozone Depletion (WMO, 2014).

[e] Very low values are not listed.

(~32%) of CCl$_4$ suggests its sources in this region. Significant enhancement was observed for CH$_3$Br with median concentrations of 31 (winter-spring) and 15 (summer) ppt, compared to the NH background of 7 ppt. Recent research showed that the natural oceanic source is now comparable to the oceanic sink (WMO, 2014). So, the abundance of CH$_3$Br in the YelRD region may be influenced by freshwater wetlands and coastal saltmarshes (WMO, 2014). This is also supported by the wind direction analysis which will be discussed later. Being widely used as refrigerants and foam blowing agents, HCFCs and HFC-134a (MP under control species) showed a dramatic increase in developing countries in the past years (Kim et al., 2011). Enhancements of HCFCs were moderate (ranging from approximately 41 to 70%) in this study,
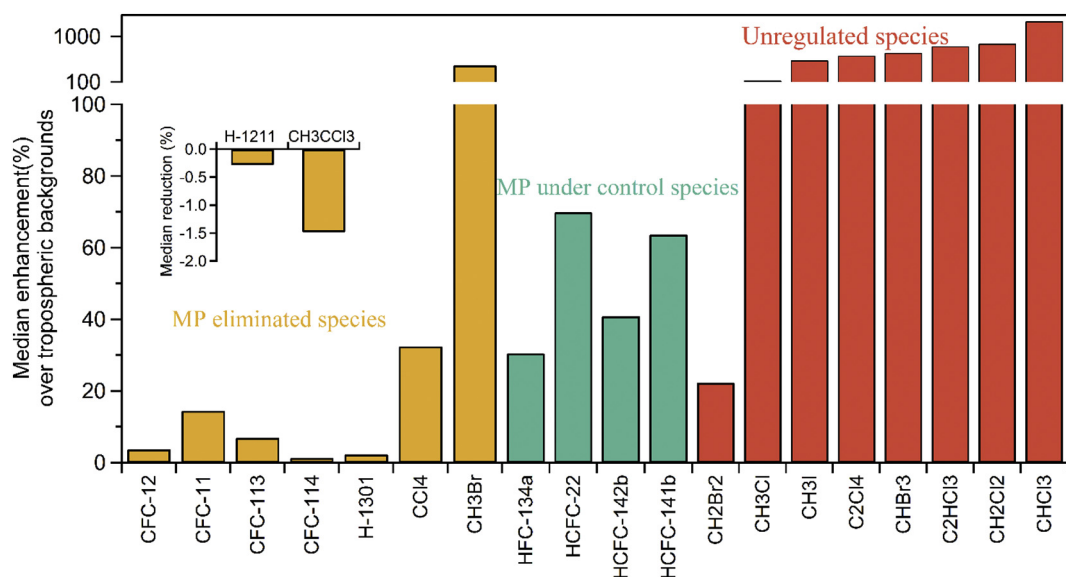

Fig. 2. Median enhancement of each halocarbon species compared with the NH background in the YelRD region.

due to the fact that their stepwise phase-out has been in force since 2013 in China. The rest chlorinated and brominated halocarbons are not regulated by MP and are categorized as unregulated species. Their enhancements were significant (ranging from approximately 20% to 2100%), indicating strong natural and/or anthropogenic sources in this region as their lifetime is relatively short.

Seasonality appears in some halocarbons due to differences in meteorological conditions, OH radical levels, and boundary layer height (Wang et al., 2005). Table 1 shows that mixing ratios of MP eliminated species (except CH_3Br) exhibited no seasonal differences because they possess a long lifetime and have been eliminated for 10 years. Wingenter et al. (1998) reported that the lowest concentrations of CH_3Br were observed in summer in the Northern Hemisphere. CH_3Br mixing ratios were also found to be lower in summer (the median was 13.5 ppt lower than that in winter-spring) in this study. This could be caused by the strengthening of its sinks in the summertime. First, reaction with OH is the dominant removal pathway of CH_3Br in the troposphere and the removal rate is lower in the winter-spring period (Blake et al., 1997). Second, there is more additional loss of CH_3Br in summer, which includes photolysis and soil microbial degradation (Wingenter et al., 1998; WMO, 2014). HCFCs (HCFC-22 and HCFC-142b) and HFC-134a concentrations were higher in summer, which was probably due to the extensive use of air conditioning. CH_3Cl levels were higher in summer as a result of biomass burning (Xue et al., 2011). CH_2Cl_2, C_2HCl_3 and C_2Cl_4 are widely used in industry as solvents and degreaser (Sturrock, 2002) and exhibited lower concentrations in the winter-spring period. This is contrary to the previous studies which reported higher concentrations of these species in winter (Artuso et al., 2010; Wang et al., 2005; Wingenter et al., 1998). This difference may be caused by the emission control policy in China. To prevent severe haze pollution, many factories, including electronic factories, PCB factories etc., were required to reduce production in winter until next spring. Marine is the major source of CH_3I. Mixing ratios of CH_3I were found to be higher in summer because of higher sea surface temperature and the summer monsoon which brought more marine air to the sampling site (Yokouchi et al., 2011). In summary, due to the influences of chemistry, meteorological conditions and emissions, some halocarbons exhibited an obvious seasonality in the YelRD region.

Comparing data collected at the sampling site with those in the oil fields and refinery, mixing ratios of most halocarbons were comparable (Table 1). Because oil production, transport and refining processes did not use or produce halocarbons, the influence of oil fields and refinery on these species was minor. For MP eliminated species (except CH_3Br which was lower in the oil fields), concentrations at the site and in the oil fields were similar, indicating an even distribution. But owing to the fact that oil fields are adjacent to Kenli District, some industrial and terrestrial biogenic source species, such as HCFC-22, HCFC-141b, CH_2Cl_2, and CH_3Cl, exhibited higher levels in the oil field samples with enhancements ranging from 13% to 29%. Meanwhile, because the oil fields are 25 km further from the Bohai Sea than the sampling site, levels of some marine source species ($CHCl_3$, CH_2Br_2, $CHBrCl_2$, $CHBr_2Cl$ and $CHBr_3$) were lower in the oil fields, ranging from 14 to 33%. Comparison of halocarbon levels in different locations reflects the fact that the oil extraction and refining should not be an important source of halocarbon compounds.

Wind sectors combined with halocarbon levels can provide insights into the local sources at a small scale. Eight species of halocarbons are presented in Fig. 3 to demonstrate the impacts of local sources. The predominant wind was from the south during the whole study period. Concentrations of CFC-12 (representative of CFCs, Fig. 3a), Halons and CH_3CCl_3 (figures not shown) were not affected by wind directions, indicating that they were from the residues in the atmosphere rather than local emissions. CH_2Cl_2, $CHCl_3$ and CH_3Cl (Fig. 3b-d), together with $CHBr_2Cl$, $CHBrCl_2$, $CHBr_3$, $C_2H_4Cl_2$ and CCl_4 (figures not shown), showed the highest values in the S-SW and S-SE sectors, suggesting the influence of the upwind urban areas to the south and/or the Bohai Sea

to the southeast. Their regional sources include marine, marine biogenic, biomass burning and industrial solvents (Chan and Chu, 2007; Simmonds et al., 1998; Wadden et al., 1991). C_2HCl_3, C_2Cl_4 and HCFC-22, species that have been widely used in industry applications, such as metal degrease, solvents, and refrigerants (Simmonds et al., 1998; Wadden et al., 1991), exhibited peak values in the W-SW and S-SW sectors. These results suggest the impacts of regional sources, especially the ones associated with the southwest sector where Dongying City, Kenli District and Huanghekou Town are located, on many halocarbons at the study site. Peak levels of CH_3I (Fig. 3h), CH_3Br and CH_2Br_2 (figures not shown) appeared in the S-SE sector and they might be influenced by freshwater wetlands, coastal saltmarshes and the Bohai Sea (WMO, 2014).

Fig. 4 demonstrates the diurnal variations of halocarbons in the two sampling periods. As presented in Fig. 4a, the MP eliminated species (except CCl_4) showed negligible variations because they have been phased out for 10 years in China. CCl_4 showed slight diurnal variations and exhibited its maximum (141.1 ppt) and minimum (116.3 ppt) at 12:00 and 18:00 LT, respectively. This suggests the existence of CCl_4 sources in this region. In Fig. 4b, the MP under control species showed higher levels in nighttime or early morning. Meanwhile, variations of these species were negligible from 9:00 to 18:00 LT. This is because these species have regional sources and would accumulate at night due to the lower boundary layer height (Guo et al., 2009). Fig. 4c exhibits the diurnal variations of CH_3Br and some unregulated species. Mixing ratios of these species showed the maximum and minimum in the morning and afternoon, respectively. This should be associated with their strong local sources and the evolution of the boundary layer height.

China has experienced dazzling economic booming during the past decades and the implementation of Montreal Protocol has been effective at the same time. Thus, various halocarbons exhibited quite different historical varieties for both reasons. Fig. 5 shows the varieties of some halocarbons in China, with different regions plotted in various colours. Up to now, CFC-11, CFC-12, CFC-113, CCl_4, CH_3CCl_3 showed a decline of 4.2, 6.6, 1.2, 1.3 and 4.2 ppt per year since 2000, respectively. The corresponding decline rates of the NH background were 1.8, 1.7, 0.7, 1.1 and 2.5 ppt per year. The production of these species should have been totally banned for about 10 years in China and their decline rates were 1.2 to 3.9 times faster than the NH background, indicating effective implementation of MP by the Chinese Government. CFC-114 is restrictively applied as propellant and refrigerant but rarely used in China with an estimated emission of 0.1 ± 0.02 Gg/yr for 2008–2009 in the PRD region (Wu et al., 2018; Zhang et al., 2014). It has a small variation with a rate of 0.1 and -0.03 ppt/yr for China and the NH background, respectively. With some exemption applications, CH_3Br exhibited an increase of 0.3 and 0.1 ppt/yr for China and the NH background, respectively. Meanwhile, increase rates of HCFC-22 (8.3 ppt/yr), HCFC-141b (0.9 ppt/yr), HCFC-142b (0.1 ppt/yr) and HFC-134a (4.4 ppt/yr) indicate wide applications and notable emissions of these species in China. NH background of these species showed a similar tendency but with lower values. For unregulated species, they did not show nationwide consistency because their lifetimes are relatively short and emissions vary significantly from region to region.

3.2. Air mass classification and its impacts on halocarbons

Backward trajectories were computed by the HYSPLIT model to understand regional transport of halocarbons for the summer and winter-spring periods. Mixing ratios of halocarbons associated with different air mass clusters were used to analyse the impacts of their source regions.

As shown in Fig. 6a, summertime air masses were grouped into four clusters, i.e. East China (EC) air mass, Northeast China (NEC) air mass, Siberia air mass and South China Sea (SCS) air mass. EC air mass occupied an overwhelming proportion of 60% due to the East Asia
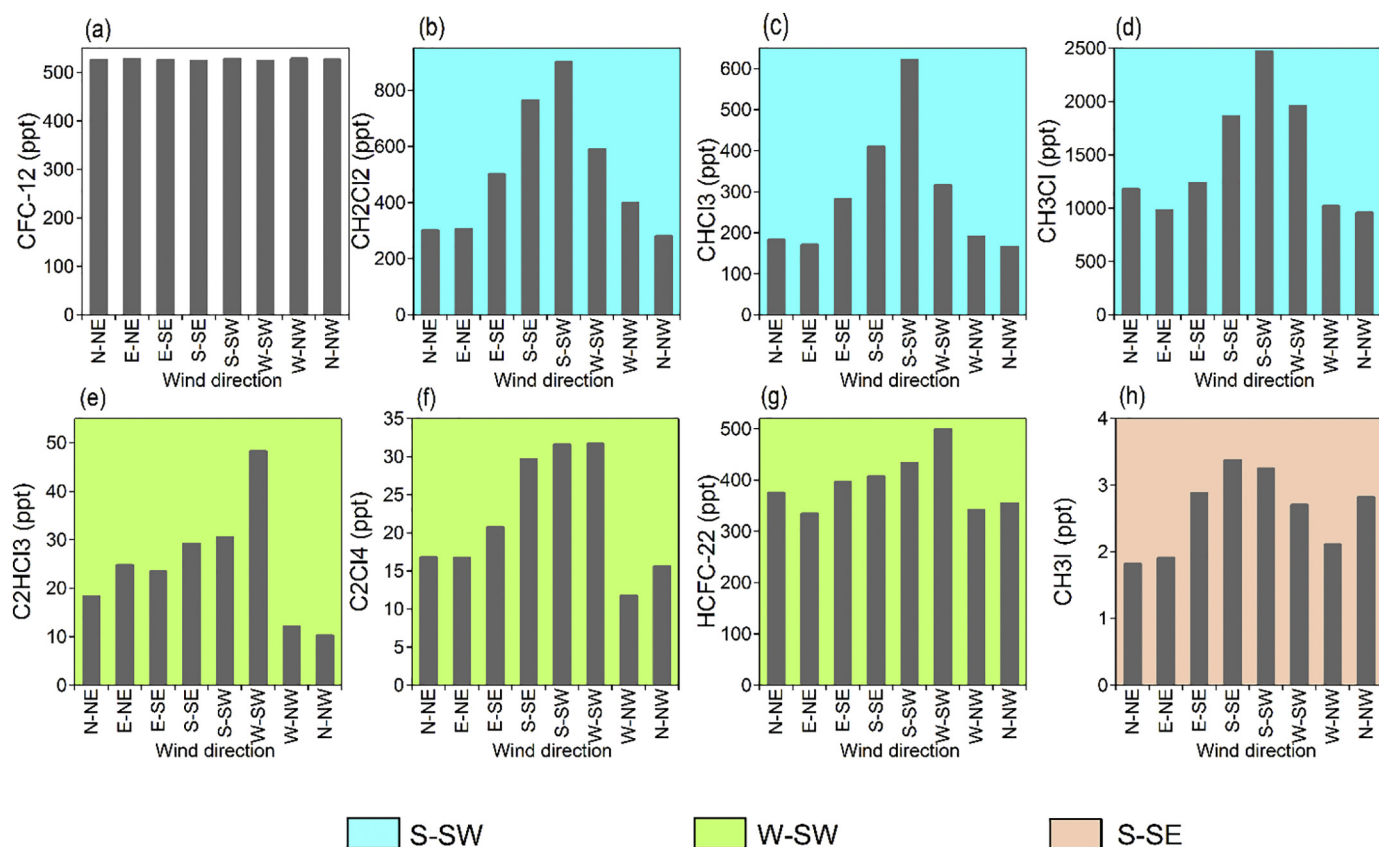
Fig. 3. Mixing ratios of halocarbons in different wind sectors. Background colours represent the corresponding wind sectors with highest concentration of halocarbons. A white background indicates concentrations of the species do not vary significantly among different sectors.
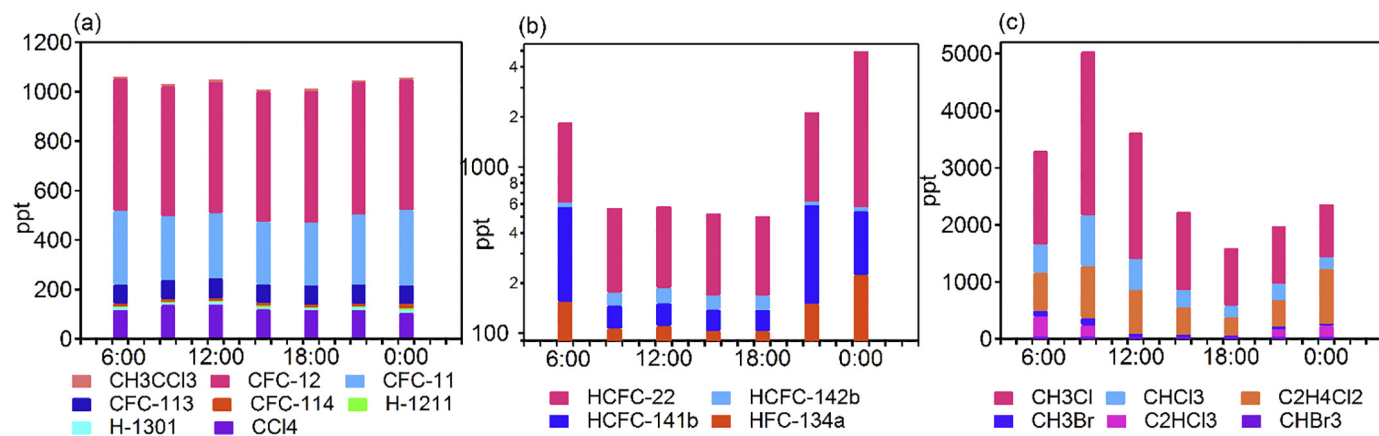

Fig. 4. Diurnal variations of (a) MP eliminated species, (b) MP under control species, and (c) unregulated species in the YelRD region.

summer monsoon. NEC, SCS and Siberia air masses accounted for 26%, 9% and 4%, respectively. SCS and Siberia air masses originated from thousand kilometres away with a faster speed, while EC and NEC air masses convoluted in small ranges and moved slowly. Fig. 6b shows, in the winter-spring period, Siberia, North China Plain (NCP) and Central Asia (CA) air masses split the trajectories with proportions of 53%, 34% and 12%, respectively. Due to Mongolia high pressure, Siberia and CA air masses came from the distant northwest, while the slowly-moving NCP air mass hovered over the polluted NCP region before reaching the site.

Median mixing ratios and standard deviations of halocarbons associated with each cluster are presented in Fig. 6c–d. Summertime Siberia air mass only contained 2 samples and was excluded from discussion. Compared with the NEC air mass, air originated from EC and

SCS loaded higher levels of most halocarbon species. The coefficient of variation (CV) of CFCs, Halons and CH_3CCl_3 in these three air masses were between 0.005 and 0.05, indicating low measures of dispersion and suggesting they have distributed evenly in the atmosphere. Comparing the halocarbon levels in the EC, NEC and SCS air masses, concentrations of some industrial species (HCFCs, HFC-134a, C_2HCl_3, C_2Cl_4, $C_2H_4Cl_2$) were on average 60% higher in the EC air mass. Meanwhile, levels of marine species (e.g., CH_3I, CH_2Br_2, $CHBrCl_2$, $CHBr_2Cl$, $CHBr_3$) were on average 52% higher in the SCS air mass. The vertical height variations of air masses provide information about the vertical mixing and pollutant accumulation processes. All air masses showed low speed and altitude before arriving at the sampling site. Such movement indicates weak turbulence diffusion and is favourable for accumulation of air pollutants. These air masses were much more
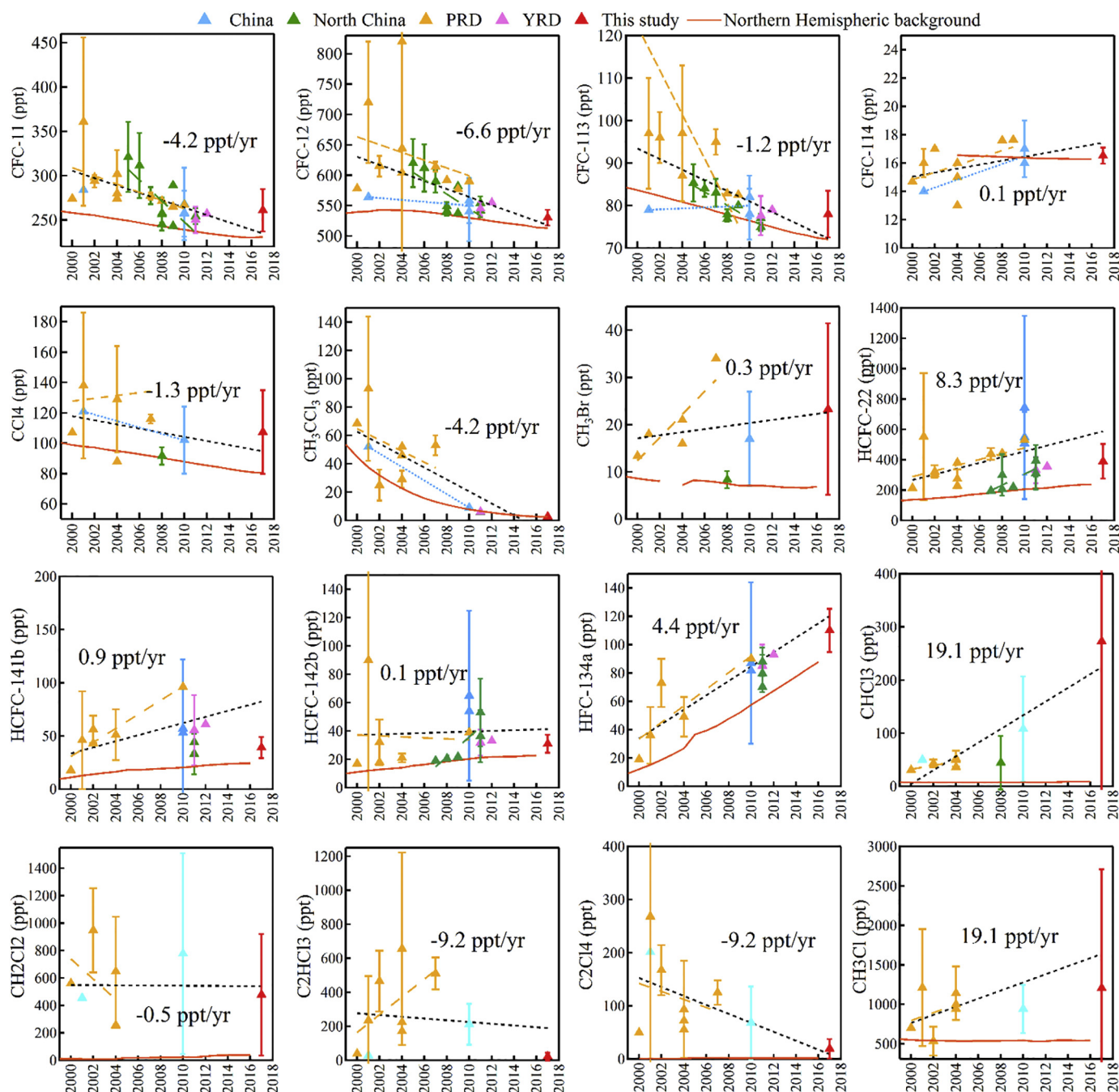
Fig. 5. Historical trends of selected halocarbons in China. Dashed lines represent curve fitting of annual variety for different regions. The NH background is the average of three sites (Trinidad Head, Mace Head and Junfraujoch). Data are the average values. But for the YelRD region, they are presented by the median to minimize the influences of extreme points. Historical data are from previous studies (An et al., 2012a; An et al., 2012b; Barletta et al., 2006; Chan et al., 2006; Chan and Chu, 2007; Chang et al., 2008; Fang et al., 2016; Fang et al., 2012a; Guo et al., 2009; Qin, 2007; Shao et al., 2011; Wang et al., 2014b; Wu et al., 2014; Wu et al., 2013; Yao et al., 2012a; Yao et al., 2012b; Zhang et al., 2010; Zhang et al., 2017; Zhang et al., 2014).

influenced by Jiangsu, Shandong and Hebei provinces. The EC air mass originated from the East China and slowly hovered above Jiangsu and Shandong provinces at altitudes below 1000 m before reaching the site. Thus, the EC air mass was well mixed with some industrial species when passing though these regions. The SCS air mass also passed though the south of Shandong Province with a low altitude below 1000 m, but it might not mix much with local pollutants due to the fast speed. Thus, the SCS air mass only carried some higher levels of marine species originating from the South China Sea. The NEC air mass slowly passed through the Bohai Sea and north of Shandong Province at altitudes below 2000 m before reaching the site. Compared with the

southern area of Shandong Province, the Bohai Sea and the northern part of Shandong were relatively clean. So the NEC air mass carried the lowest levels of halocarbons of all three air masses.

In the winter-spring period, the NCP air mass dominated the pollutants of clusters. Concentrations of CFCs, Halons and CH_3CCl_3 were similar in different air masses, while mixing ratios of the rest species were on average 80% higher in the NCP air mass. The NCP air mass moved slowly in the polluted NCP region at altitudes below 2000 m, leading to strong accumulation of air pollutants in the boundary layer. This plume had strong regional influence and brought high levels of halocarbons to the YelRD region. In contrast, the Siberia and CA air
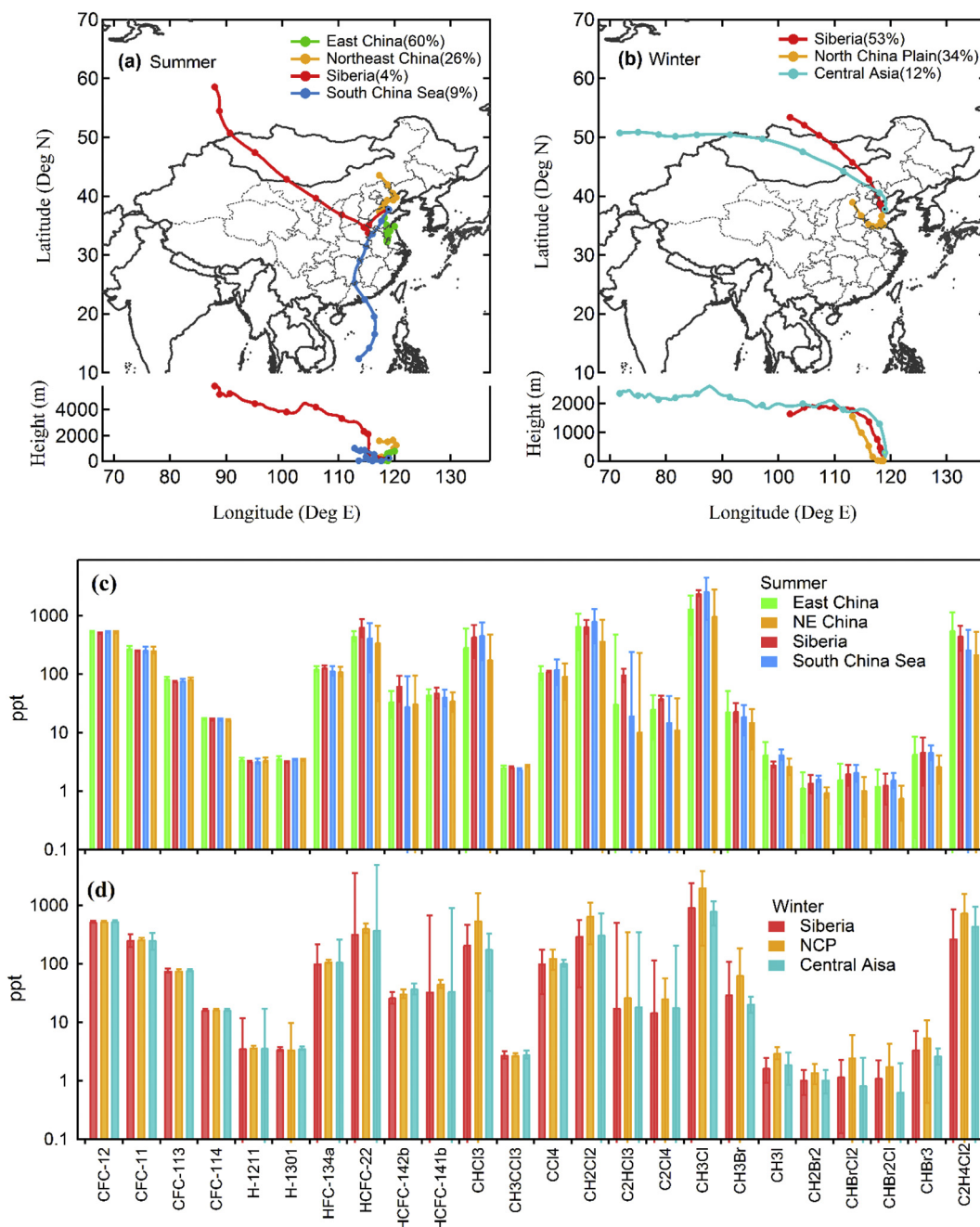
Fig. 6. Five-day HYSPLIT back trajectory clusters and comparison of the associated concentrations of halocarbons in the YelRD region. (a), (c) and (b), (d) stand for summer and winter-spring, respectively. Levels of halocarbons are presented with median ± SD.

masses originated from Central Asia at an altitude of 2000 m and moved fast along the pathway. Thus, they carried the lowest levels of pollutants.

Overall, the backward trajectory cluster and air mass load show that the North China Plain and East China region were the main source regions of halocarbons that affected the YelRD in winter-spring and summer, respectively.

3.3. Source apportionment analysis

Fig. 7 shows the mean source profiles and contributions of each source derived from PMF. Five types of sources were finally identified according to goodness of fit to the data and prior knowledge.

The first source was characterized by high loadings of CH_3Cl and identified as biomass burning (Xue et al., 2011). About 84% of CH_3Cl

was from this source. Biomass burning is also proposed as a minor source of $CHCl_3$ and CH_2Cl_2 (Sarkar et al., 2018). And indeed about 24% of $CHCl_3$ and 20% of CH_2Cl_2 originated from this source in this study.

The second source was distinguished as solvent usage. Its profile is mainly made up with high mass fractions of C_2HCl_3 (75%) and C_2Cl_4 (67%). C_2HCl_3 is primarily used as surface degreaser agent and solvent in electronic and textile industrial processes (Simmonds et al., 1998). C_2Cl_4 is widely used as industrial cleaning solvents in electronic industry (Guo et al., 2009). In addition, as shown in Fig. 3, the most polluted air masses of C_2Cl_4 and C_2HCl_3 were from the southwest (Dongying City) where some electronic and cleaning factories were located. C_2Cl_4 and C_2HCl_3 also showed a good correlation with each other (r = 0.7).

The third source was characterized as refrigerants and foam blowing
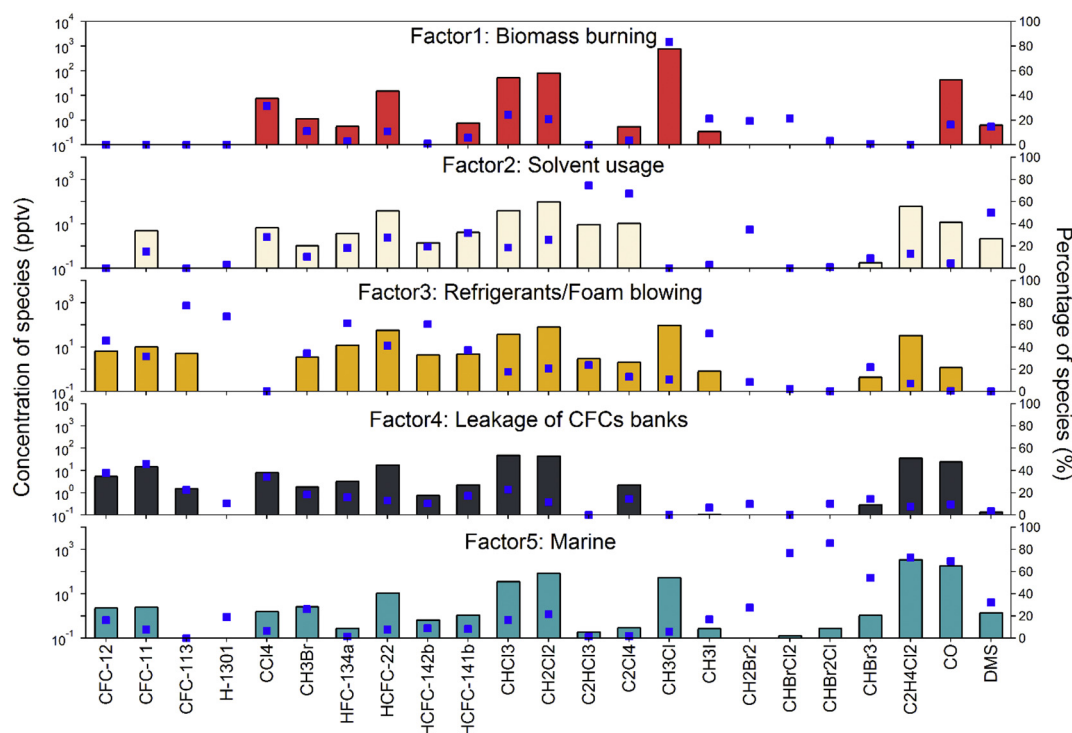
Fig. 7. Source profiles resolved from PMF in the YelRD region (results represent the average of the summer and winter-spring time periods).

by high mass percentages of HCFCs (HCFC-22, HCFC-141b and HCFC-142b), HFC-134a, and CFC-113. HCFC-22, HFC-134a and HCFC-142b are major refrigerant replacements in post-MP era (posterior to the signing of the Montreal Protocol). HCFC-22 is widely used in commercial refrigeration and refrigeration transport. HFC-134a is commonly applied in mobile air conditioning system (McCulloch et al., 2003). HCFC-142b is mainly used in air conditioning system in high-temperature environment and as a blowing agent (Simmonds et al., 1998). Meanwhile, HCFC-141b is primarily used as foam blowing agents in the manufacture of shoes and motor dashboards, and it also used as cleaning fluids for electrical equipment (Derwent et al., 2007). CFC-113 is mainly used as refrigerant and cleaning solvents in leather making and electronic industry (Fraser et al., 1996). There are many refrigeration plants and leather shoes factories in the YelRD region. In addition, with the rapid economic development, air conditioners and private vehicles become commonplace in this region, which are strong sources of HCFCs and HFC-134a species.

Leakage of CFCs banks were identified as the forth source for high proportions of CFC-11, CFC-12, CFC-113 and CCl4. These compounds have been phased-out for about 10 years in China (Aucott et al., 1999; McCulloch and Midgley, 2001; McCulloch et al., 2003). However, CFCs and CCl4 produced in the pre-MP era are stored in equipment and products and can leak into the environment.

The last source is marine air. This source is associated with high mass percentage of DMS, CHBr3, CHBrCl2, CHBr2Cl and CH2Br2. These species are typically used as ocean tracers (Cox et al., 2003; Sarkar et al., 2018). They showed good correlation with each other (with r ranging from 0.28 to 0.97), indicating they are from marine and marine biogenic sources.

Based on the PMF analysis, average contributions of each factor to the total halocarbons are illustrated in Fig. 8a. It can be seen that biomass burning (37%) and marine (23%) are two major contributors in this region. Refrigerants and foam blowing, solvent usage, and leakage of CFCs banks contributed 15%, 15% and 10%, respectively. Wheat straw burning can make significant contributions to halocarbons in summer as many farmlands exist in this region. The Bohai Sea is close to the YelRD region, and the influence of it on total halocarbons levels

was also high. Compared with developed regions (the PRD, Singapore, South Korea), local industry of this area is relatively underdeveloped and showed much lower contributions (Guo et al., 2009; Li et al., 2014; Sarkar et al., 2018).

Considering the seasonal difference, PMF was also conducted separately for the summer and winter-spring periods. The results are shown in Fig. 8b and c. In the winter-spring period, five sources, namely, biofuel burning (39%), marine (32%), solvent usage (15%), refrigerants and foam blowing (8%), leakage of CFCs banks (6%) were identified. It is worth noting that biofuel burning was identified as the largest source in the profile with high percentage of CH3Cl (80%) and CO (49%). This source is the results of biofuel/biomass burning in northern China for residential heating in winter. While other sources had similar proportions to the above-identified overall source profiles. In summertime, biomass burning, refrigerants and foam blowing were major sources of halocarbons with proportions of 33% and 29%, respectively. Meanwhile, marine, solvent usage, and leakage of CFCs banks contributed 19%, 6% and 13%, respectively. The high proportions of biomass burning and refrigerants can be explained by wheat straw burning and air conditioning in summer. PMF results reveal that halocarbons in the YelRD region were mainly influenced by biomass (biofuel) burning, marine air and refrigerants.

4. Conclusions

A two-phase field campaign was conducted in the YelRD area which is China's second largest estuary delta region. Halogenated hydrocarbons samples were collected at a rural site and in the oil fields in winter-spring and summer 2017. Concentrations of major MP eliminated species at the sampling site were comparable to the NH background, indicating the implementation of MP is effective in China. The high enhancement of CH3Br might be the result of the emissions from freshwater wetlands and coastal saltmarshes. Meanwhile, enhancements of MP under control species (HCFCs and HFC-134a) and unregulated species were moderate and significant. Oil production, transport and refining processes were found to have negligible influences on halocarbon levels at the site. Seasonal and diurnal varieties of
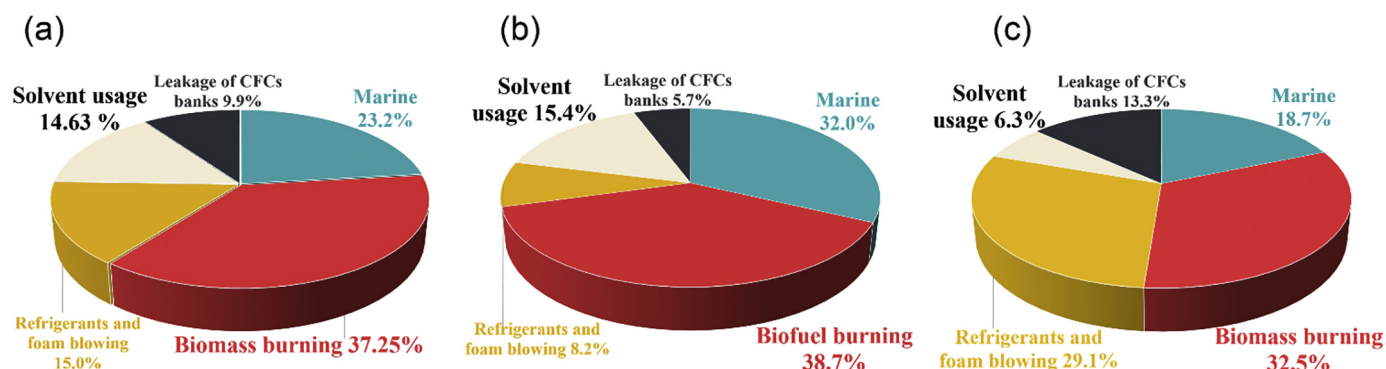
Fig. 8. Source contributions to the total halocarbons in the YelRD region: (a) overall source contributions, (b) winter-spring period, and (c) summer period.

halocarbons in each category were different. The factors that led to those discrepancies were chemical lifetime, emission and meteorology differences as well as different phase-out schedules under the Montreal Protocol. Historical data show that in China, levels of regulated species exhibited a declining trend while concentrations of MP under control species showed an increasing trend. Back trajectory analysis indicates air masses from the North China Plain and East China loaded the highest concentrations of most halocarbons during the winter-spring and summer periods, respectively. PMF model results show that biofuel burning and biomass burning were the most major sources of total halocarbons in winter-spring and summer, respectively. Refrigerants and foam blowing, solvent usage, leakage of CFCs banks and marine air are also important sources of halocarbons in this region. This study demonstrates effective emission reductions of most MP eliminated species in China, and calls for further efforts to control the CFCs replacements and short-lived halocarbons.

Acknowledgments

Appendix A. Supplementary data

Supplementary data to this article can be found online at https://doi.org/10.1016/j.atmosres.2019.03.039.

References

An, X.Q., et al., 2012a. Estimating emissions of HCFC-22 and CFC-11 in China by atmospheric observations and inverse modeling. Sci. China Chem. 55, 2233–2241.

An, X.Q., Zhou, L.X., Yao, B., Xu, L., Ma, L., 2012b. Analysis on source features of halogenated gases at Shangdianzi regional atmospheric background station. Atmos. Environ. 57, 91–100.

Artuso, F., et al., 2010. Tropospheric halocompounds and nitrous oxide monitored at a remote site in the Mediterranean. Atmos. Environ. 44, 4944–4953.

Aucott, M.L., et al., 1999. Anthropogenic emissions of trichloromethane (chloroform, CHCl3) and chlorodifluoromethane (HCFC-22): reactive chlorine emissions inventory. J. Geophys. Res.-Atmos. 104, 8405–8415.

Barletta, B., et al., 2006. Ambient halocarbon mixing ratios in 45 Chinese cities. Atmos.

Environ. 40, 7706–7719.

Blake, N.J., et al., 1997. Distribution and seasonality of selected hydrocarbons and halocarbons over the western Pacific basin during PEM-West A and PEM-West B. J. Geophys. Res.-Atmos. 102, 28315–28331.

Chan, L.Y., Chu, K.W., 2007. Halocarbons in the atmosphere of the industrial-related Pearl River Delta region of China. J. Geophys. Res. 112.

Chan, C.Y., Tang, J.H., Li, Y.S., Chan, L.Y., 2006. Mixing ratios and sources of halocarbons in urban, semi-urban and rural sites of the Pearl River Delta, South China. Atmos. Environ. 40, 7331–7345.

Chang, C.-C., et al., 2008. Variability of ozone depleting substances as an indication of emissions in the Pearl River Delta, China. Atmos. Environ. 42, 6973–6981.

Colman, J.J., et al., 2001. Description of the analysis of a wide range of volatile organic compounds in whole air samples collected during PEM-Tropics A and B. Anal. Chem. 73, 3723–3731.

Cox, M.L., et al., 2003. Regional sources of methyl chloride, chloroform and dichloromethane identified from AGAGE observations at Cape Grim, Tasmania, 1998–2000. J. Atmos. Chem. 45, 79–99.

Draxier, R.R., Hess, G.D., 1998. An overview of the HYSPLIT_4 modelling system for trajectories, dispersion and deposition. Aust. Meteorol. Mag. 47, 295–308.

Derwent, R.G., et al., 2007. The phase-in and phase-out of European emissions of HCFC-141b and HCFC-142b under the Montreal protocol: evidence from observations at Mace Head, Ireland and Jungfraujoch, Switzerland from 1994 to 2004. Atmos. Environ. 41, 757–767.

EPA, U, 2014. EPA Positive Matrix Factorization (PMF) 5.0 Fundamentals and User Guide.

Fang, X., et al., 2012a. Estimates of major anthropogenic halocarbon emissions from China based on interspecies correlations. Atmos. Environ. 62, 26–33.

Fang, X., et al., 2012b. Ambient mixing ratios of chlorofluorocarbons, hydrochlorofluorocarbons and hydrofluorocarbons in 46 Chinese cities. Atmos. Environ. 54, 387–392.

Fang, X., et al., 2016. Hydrofluorocarbon (HFC) emissions in China: an inventory for 2005-2013 and Projections to 2050. Environ. Sci. Technol. 50, 2027–2034.

Fang, X., et al., 2018a. Rapid increase in ozone-depleting chloroform emissions from China. Nat. Geosci. 12, 89–93.

Fang, X., et al., 2018b. Changes in emissions of ozone-depleting substances from China due to implementation of the Montreal protocol. Environ. Sci. Technol. 52, 11359–11366.

Fraser, P., et al., 1996. Lifetime and emission estimates of 1,1,2-trichlorotrifluorethane (CFC-113) from daily global background observations June 1982 June 1994. J. Geophys. Res.-Atmos. 101, 12585–12599.

Guo, H., et al., 2009. Source origins, modeled profiles, and apportionments of halogenated hydrocarbons in the greater Pearl River Delta region, southern China. J. Geophys. Res. 114.

IPCC/TEAP, 2005. IPCC/TEAP Special Report on Safeguarding the Ozone Layer and the Global Climate System: Issues Related to Hydrofluorocarbons and Perfluorocarbons.

Kim, K.-H., Shon, Z.-H., Nguyen, H.T., Jeon, E.-C., 2011. A review of major chlorofluorocarbons and their halocarbon alternatives in the air. Atmos. Environ. 45, 1369–1382.

Li, S., et al., 2014. Source identification and apportionment of halogenated compounds observed at a remote site in East Asia. Environ. Sci. Technol. 48, 491–498.

Lunt, M.F., et al., 2018. Continued emissions of the ozone-depleting substance carbon tetrachloride from Eastern Asia. Geophys. Res. Lett. 45, 11,423–411,430.

McCulloch, A., Midgley, P.M., 2001. The history of methyl chloroform emissions: 1951–2000. Atmos. Environ. 35 (1994), 5311–5319.

McCulloch, A., Midgley, P.M., Ashford, P., 2003. Releases of refrigerant gases (CFC-12, HCFC-22 and HFC-134a) to the atmosphere. Atmos. Environ. 37, 889–902.

Molina, M.J., Rowland, F.S., 1974. Stratospheric sink for chlorofluoromethanes: chlorine atomic-catalysed destruction of ozone. Nature 249, 810–812.

Montzka, S.A., Butler, J.H., Elkins, J.W., Thompson, T.M., Clarke, A.D., 1999. Present and future trends in the atmospheric burden of ozone-depleting halogens. Nature (London) 398, 690–694.

Montzka, S.A., et al., 2018. An unexpected and persistent increase in global emissions of ozone-depleting CFC-11. Nature 557, 413–417.

O'Doherty, S., et al., 2001. In situ chloroform measurements at Advanced Global Atmospheric Gases Experiment atmospheric research stations from 1994 to 1998. J.

Geophys. Res.-Atmos. 106, 20429–20444.

O'Doherty, S., et al., 2004. Rapid growth of hydrofluorocarbon 134a and hydrochloro-fluorocarbons 141b, 142b, and 22 from Advanced Global Atmospheric Gases Experiment (AGAGE) observations at Cape Grim, Tasmania, and Mace Head, Ireland. J. Geophys. Res.-Atmos. 109 (pp. n/a-n/a).

Qin, D., 2007. Decline in the concentrations of chlorofluorocarbons (CFC-11, CFC-12 and CFC-113) in an urban area of Beijing, China. Atmos. Environ. 41, 8424–8430.

Sarkar, S., et al., 2018. A quantitative assessment of distributions and sources of tropospheric halocarbons measured in Singapore. Sci. Total Environ. 619-620, 528–544.

Shao, M., et al., 2011. Estimate of anthropogenic halocarbon emission based on measured ratio relative to CO in the Pearl River Delta region, China. Atmos. Chem. Phys. 11, 5011–5025.

Simmonds, P.G., et al., 1998. Calculated trends and the atmospheric abundance of 1,1,1,2-tetrafluoroethane, 1,1-dichloro-1-fluoroethane, and 1-chloro-1,1-difluoroethane using automated in-situ gas chromatography-mass spectrometry measurements recorded at Mace Head, Ireland, from Octob. J. Geophys. Res.-Atmos. 103, 16029–16037.

Simmonds, P.G., et al., 2006. Global trends, seasonal cycles, and European emissions of dichloromethane, trichloroethene, and tetrachloroethene from the AGAGE observations at Mace Head, Ireland, and Cape Grim, Tasmania. J. Geophys. Res. 111.

Simpson, I.J., et al., 2010. Characterization of trace gases measured over Alberta oil sands mining operations: 76 speciated C-2-C-10 volatile organic compounds (VOCs), CO2, CH4, CO, NO, NO2, NOy, O-3 and SO2. Atmos. Chem. Phys. 10, 11931–11954.

Stohl, A., et al., 2003. A backward modeling study of intercontinental pollution transport using aircraft measurements. J. Geophys. Res.-Atmos. 108.

Sturrock, G.A., 2002. Atmospheric histories of halocarbons from analysis of Antarctic firn air: major Montreal protocol species. J. Geophys. Res. 107.

Sun, L., et al., 2016. Significant increase of summertime ozone at Mount Tai in Central Eastern China. Atmos. Chem. Phys. 16, 10637–10650.

Wadden, R.A., Hawkins, J.L., Scheff, P.A., Franke, J.E., 1991. Characterization of emission factors related to source activity for trichloroethylene degreasing and chrome plating processes. Am. Ind. Hyg. Assoc. J. 52, 349–356.

Wang, T., et al., 2005. Measurements of trace gases in the inflow of South China Sea background air and outflow of regional pollution at Tai O, Southern China. J. Atmos. Chem. 52, 295–317.

Wang, C., et al., 2014a. Estimating halocarbon emissions using measured ratio relative to

tracers in China. Atmos. Environ. 89, 816–826.

Wang, Y.H., et al., 2014b. Ozone weekend effects in the Beijing–Tianjin–Hebei metropolitan area, China. Atmos. Chem. Phys. 14, 2419–2429.

Wingenter, O.W., Wang, C.J.L., Blake, D.R., Rowland, F.S., 1998. Seasonal variation of tropospheric methyl bromide concentrations: constraints on anthropogenic input. Geophys. Res. Lett. 25, 2797–2800.

WMO, 2014. Scientific assessment of ozone depletion: 2014.

WMO, 2018. Scientific Assessment of Ozone Depletion 2018 Excutive Summary.

Wu, J., et al., 2013. Chlorofluorocarbons, hydrochlorofluorocarbons, and hydrofluorocarbons in the atmosphere of four Chinese cities. Atmos. Environ. 75, 83–91.

Wu, J., et al., 2014. Estimated emissions of chlorofluorocarbons, hydrochlorofluorocarbons, and hydrofluorocarbons based on an interspecies correlation method in the Pearl River Delta region, China. Sci. Total Environ. 470-471, 829–834.

Wu, H., Chen, H., Wang, Y., Ding, A., Chen, J., 2018. The changing ambient mixing ratios of long-lived halocarbons under Montreal Protocol in China. J. Clean. Prod. 188, 774–785.

Xue, L., et al., 2011. Vertical distributions of non-methane hydrocarbons and halocarbons in the lower troposphere over Northeast China. Atmos. Environ. 45, 6501–6509.

Yao, B., et al., 2012a. Sampling-analysis-quality control method for atmospheric hydrofluorocarbons (HFCs). China Environ. Sci. 32, 1597–1601.

Yao, B., et al., 2012b. A study of four-year HCFC-22 and HCFC-142b in-situ measurements at the Shangdianzi regional background station in China. Atmos. Environ. 63, 43–49.

Yokouchi, Y., Saito, T., Ooki, A., Mukai, H., 2011. Diurnal and seasonal variations of iodocarbons (CH2ClI, CH2I2, CH3I, and C2H5I) in the marine atmosphere. J. Geophys. Res. 116.

Zhang, F., et al., 2010. Analysis of 3-year observations of CFC-11, CFC-12 and CFC-113 from a semi-rural site in China. Atmos. Environ. 44, 4454–4462.

Zhang, Y.L., et al., 2014. Ambient CFCs and HCFC-22 observed concurrently at 84 sites in the Pearl River Delta region during the 2008-2009 grid studies. J. Geophys. Res.-Atmos. 119, 7699–7717.

Zhang, G., et al., 2017. Ambient mixing ratios of atmospheric halogenated compounds at five background stations in China. Atmos. Environ. 160, 55–69.

Zhang, Y., et al., 2019. Observations of C1–C5 alkyl nitrates in the Yellow River Delta, northern China: effects of biomass burning and oil field emissions. Sci. Total Environ. 656, 129–139.